Soil Dynamics and Earthquake Engineering 134 (2020) 106152

Contents lists available at ScienceDirect

Soil Dynamics and Earthquake Engineering

journal homepage: http://www.elsevier.com/locate/soildyn

Liquefaction of a sloping deposit: LEAP-2017 centrifuge tests at Rensselaer Polytechnic Institute

Evangelia Korre, Tarek Abdoun, Mourad Zeghal *

Rensselaer Polytechnic Institute, Troy, NY, USA

ARTICLE INFO

Keywords:
Centrifuge modeling
Liquefaction
Dilation
Lateral displacement and sloping ground

ABSTRACT

A series of centrifuge tests of a sloping ground were conducted at Rensselaer Polytechnic Institute (RPI). These tests were used to monitor and assess the soil response, in terms of generated accelerations, excess pore water pressure (EPWP) and associated lateral spreading, as a function of variations in the dynamic input motion and soil relative density. This series of tests are part of the Liquefaction Experiments and Analysis Projects (LEAP-2017), an international effort to assess the repeatability and reproducibility of centrifuge experimental results, and verify and validate soil liquefaction numerical tools using the experimental data.

1. Introduction

Soil liquefaction during earthquakes causes significant damage and remains a challenging problem in geotechnical engineering practice and research. The mechanism of failure induced by liquefaction has been a subject of research for a number of decades [1–7]. Centrifuge testing and advanced numerical tools have been utilized to shed light on the governing mechanisms of this phenomenon. However, a lack of consistency between adopted methodologies and results at different experimental facilities prevented, in some instances, the engineering community from reaching consensus in addressing the associated problem. Furthermore, there is also a lack of consistency between the numerical tools which somewhat limits the usefulness of the associated predictions. Thus, there is a strong need for validation of these tools using high quality experimental data. For instance Ref. [8], clearly underscore that a robust practice of validating numerical methods is necessary.

In the 1990's the project VELACS (VErify Liquefaction Analyses by Centrifuge Studies) was undertaken [9]. This project was a valuable international effort of centrifuge testing among different facilities. "Blind predictions" (Type A) were performed, in an attempt to validate numerical simulations based on the centrifuge results. This initiative led to the following two observations: (a) the numerical tools available at that time showed significant shortcomings in predicting the results of liquefaction, and (b) the experimental results across the different facilities revealed significant inconsistencies [10].

Over the recent decades, there has been remarkable progress in the experimental potential of centrifuge testing. At the same time, advances in soil constitutive modeling and computational capabilities of computers created propitious conditions leading to the development of robust numerical tools, capable of simulating soil systems under complex conditions, such as in the presence of liquefaction. The Liquefaction Experiments and Analysis Projects (LEAP) is an international effort which aims at assessing and demonstrating the reliability of centrifuge testing and establishing a uniform and consistent way of verifying and validating the numerical tools of soil liquefaction using high quality experimental data. In 2017, a LEAP (referred to as LEAP-2017) was undertaken using centrifuge tests of a saturated mildly-sloping deposit. Tests were conducted at 9 different centrifuge facilities [11] and aimed at monitoring the soil response in terms of accelerations, excess pore water pressure (EPWP) and the associated permanent surficial displacements.

This paper presents and discusses the results of three centrifuge tests RPI01, RPI02 and RPI03 that were performed at CEES (Center for Earthquake Engineering Simulation) at Rensselaer Polytechnic Institute (RPI) during LEAP-2017. The group of tests aims at assessing the effects of variations in input ground motion and soil relative density on the analyzed deposit response. The first test, RPI01, was presented in detail in Ref. [12] along with other tests to provided evidence of the repeatability capabilities of the RPI facility. Herein, RPI01 is used as a reference for comparisons with the other two tests (RPI02 and RPI03). Unless otherwise stated, all dimensions and results are presented hereafter in prototype units.

* Corresponding author.
E-mail addresses: korree@rpi.edu, korre.eva@gmail.com (E. Korre), zeghal@rpi.edu (M. Zeghal).

https://doi.org/10.1016/j.soildyn.2020.106152
Received 7 November 2019; Received in revised form 19 February 2020; Accepted 23 March 2020
Available online 20 April 2020

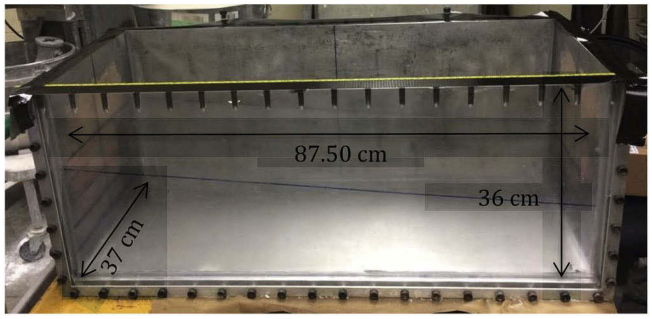

Fig. 1. The "rigid" aluminium container utilized for the conducted centrifuge experiments.

2. Experimental methodology

2.1. Equipment

The equipment at CEES comprises of a 3-m radius geotechnical centrifuge, with a loading capacity of 150 g tons. Installed on the basket of the centrifuge is a 2 degree-of–freedom shaking table. The actuators of the shaking table provide the possibility of generating artificial as well as earthquake motions within a 5% accuracy of the original prescribed ground motions.

A rectangular rigid container, made of aluminum with a plexiglass window and lid, was used to build the sloping deposit model. The associated dimensions are shown in Fig. 1. The Loading System at RPI was utilized to conduct in-flight cone penetration tests (CPTs) to characterize the deposit conditions. The Loading System capability allows movement in 2 degrees of freedom; along the z axis (vertically) and along the x axis (horizontally). The cone utilized for the CPT has a diameter of 6 mm and total length of 150 mm, which correspond to a diameter of 0.138 m and length of 3.45 m in prototype units under the 23 g gravitational field applied for RPI01, RPI02 and RPI03.

2.2. Experimental set up and instrumentation

The set up and dimensions for the LEAP-2017 experiments are shown in Fig. 2. The tested soil stratum was a 5-degree mildly sloping ground of dry Ottawa sand produced by U. S. Silica. Based on tests performed at GeoTesting Express in Acton, MA, the batch of Ottawa sand used for these experiments was found to have a minimum mass density $\rho_{min} = 1495$ kg/m^3 (with a void ratio $e_{max} = 0.773$), a maximum mass density $\rho_{max} = 1759$ kg/m^3 (with a void ratio $e_{min} = 0.507$) and specific gravity of solids $G_s = 2.65$. According to the gradation curve produced by U. S. Silica, the batch of sand utilized had the following characteristics: fines (less than 0.075 mm) = 0.3%, D10 = 0.14 mm, D30 = 0.175 mm, and D60 = 0.22 mm.

After calibration, drop heights of 7.60 cm (3 inches) and 3.80 cm (1.5 inches) were selected for the deposition to achieve relative densities of 65% (for RPI01, RPI02) and 45% (for RPI03), respectively (Table 2), using the method of air pluviation. Based on the dimensions of the container, a 23 g level was selected to perform the tests. The container was placed on the basket in such a way, so that the direction of shaking and the axis of the centrifuge are parallel. Thus, no curving of the slope surface was needed in the longitudinal direction. The surface of the slope was also not curved in the transverse direction. The width of the container is 37 cm while the centrifuge effective radius is 2.70 m. Curving the surface in the transverse direction to accommodate the centrifugal acceleration field would require about 5 mm (model units) increase in the soil height at the container wall (and lower increase towards the model center in this direction). Such a modification was deemed unnecessary.

The adopted methodology to build the model was repeated in all three tests RPI01, RPI02 and RPI03 as described in Ref. [12]. The model deposit was pluviated dry in horizontal layers of equal thickness. After pluviating each layer, detailed elevation measurements were taken in a grid of 35 points, monitoring in this way the uniformity of the achieved relative density within the stratum [12]. The sensors were buried at the designated locations within the layers.

Fig. 2 shows schematically the locations of the accelerometers, pore pressure transducers and bender elements used to monitor the model

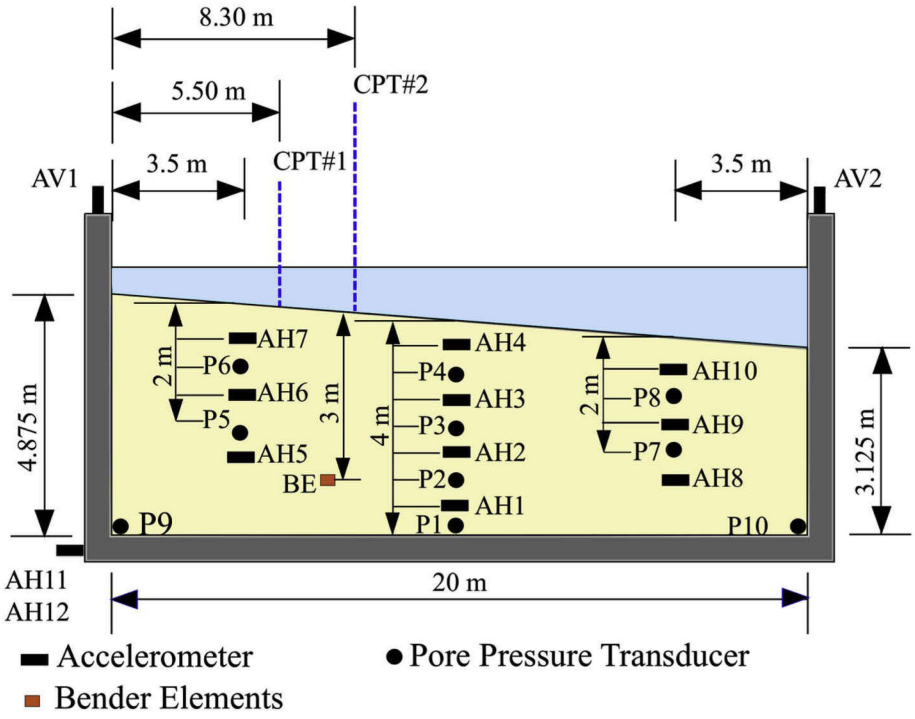

Fig. 2. The experimental set up of LEAP-2017 centrifuge tests.

Table 1
Locations of Accelerometers and Pore Water Pressure Transducers as recorded for RPI01 during construction and dissection of the model, along with the settlements (S) of the sensors as recorded for RPI01, RPI02 and RPI03 during the excavation (z* is the elevation of the sensors' locations measured from the bottom of the container).

(a) Accelerometers

	Model Construction Coordinates			Model Dissection Coordinates			S : m	S : m	S : m
Sensor	x : m	y : m	z*: m	x : m	y : m	z*: m	(RPI01)	(RPI02)	(RPI03)
AH1	0.29	−1.15	0.58	0.75	−1.27	0.58	0	0	0.02
AH2	0.17	−1.15	1.5	0.06	−1.04	1.47	0.03	0.02	0.07
AH3	−0.06	−1.15	2.53	−0.4	−1.04	2.51	0.02	0.02	0.16
AH4	−0.63	1.73	3.45	−0.4	1.73	3.43	0.02	0.02	0.35
AH5	−6.61	−0.58	2.48	−6.73	−0.58	2.44	0.04	0.07	0.16
AH6	−6.15	1.04	3.4	−6.5	1.04	3.38	0.02	0.09	0.46
AH7	−5.46	0.35	4.14	−5.58	0.58	4.12	0.02	0.14	0.6
AH8	6.73	−1.15	1.5	6.84	−1.38	1.52	−0.02	−0.02	−0.05
AH9	6.73	−0.35	2.48	6.84	−0.35	2.53	−0.05	−0.05	−0.09
AH10	6.73	−0.92	3.15	6.84	−1.27	3.22	−0.07	−0.12	−0.16
AH11	10.06	−4.26	0	N/A	N/A	N/A	N/A	N/A	N/A
AH12	10.06	4.26	0	N/A	N/A	N/A	N/A	N/A	N/A
AV1	−10.06	0	8.28	N/A	N/A	N/A	N/A	N/A	N/A
AV2	10.06	0	8.28	N/A	N/A	N/A	N/A	N/A	N/A

(b) Pore Pressure Transducers

	Model Construction Coordinates			Model Dissection Coordinates			S: m	S: m	S: m
Sensors	x: m	y: m	z*: m	x: m	y: m	z*: m	(RPI01)	(RPI02)	(RPI03)
P1	−0.52	−0.30	0.23	−0.06	−0.81	0.23	0	0.02	0.05
P2	−0.52	−0.35	1.01	−1.21	−0.35	1.01	0	0.02	0.07
P3	0.06	−0.46	2.00	−0.17	−0.58	1.95	0.05	0.07	0.09
P4	0.75	−0.35	2.99	1.09	−0.46	2.92	0.07	0.12	0.3
P5	−7.83	1.27	2.99	−7.76	1.27	2.92	0.07	0.07	0.32
P6	−6.38	0.12	4.00	−6.38	0.00	3.88	0.12	0.14	0.39
P7	6.50	0.78	2.02	6.61	0.58	2.04	−0.02	−0.02	0.07
P8	6.73	0.85	2.99	6.73	0.69	3.04	−0.05	−0.09	0.09
P9	−8.06	−0.81	0.28	−8.11	−0.92	0.26	0.02	−0.02	−0.02
P10	6.80	−0.05	0.23	6.84	−0.35	0.21	0.02	0	−0.07

Table 2
Characteristics of the RPI LEAP-2017 centrifuge models.

Experiment Name	Dr (%)	Type of Input Motion	Predominant Frequency (Hz)	a_{max} (g)
RPI01	65%	1	1	0.150
RPI02	65%	2	1 and 3	0.142
RPI03	45%	1	1	0.155

response and characteristics. Note that the bender elements were used only for RPI02 and RPI03. The accelerometers AH1 – AH10 were used to monitor the soil deposit, whereas AH11 and AH12 were mounted at the base of the rigid box to record the applied input ground motion. AV1 and AV2 were mounted at the top of the container, at mid-length of the transverse side and were used to record the vertical acceleration of the container. Pore pressure transducers P1 – P10 were installed within the stratum after an overnight saturation to ensure that no trapped air remained between the sensor and the installed filter. As a reference, Table 1 provides the as-built coordinates of the sensor locations from RPI01. For the three experiments, the locations of the sensors where replicated, with an accuracy of repeatability within 5–10%.

The two locations which were suitable to accommodate the CPT, are shown in Fig. 2. The selection was based both on the available margin in distance from neighboring sensors, and on the availability of soil depth at these two locations, so that the entire cone could penetrate the soil stratum. Wei et al. [13] showed that for a $d \geq 7.6D$, where d is the distance between the cone and the sensors and D is the diameter of the cone, the effect in the lateral earth pressure induced by the penetrating cone is not significant. In the tests discussed herein, the adopted distance from the sensors at the selected CPT locations was $d \geq 9D$. During the CPT all pore water pressure transducers were monitored and practically no pore pressure buildup was observed.

The models were sealed with the plexiglass lid, installed on the basket of the centrifuge and vacuum of approximately 26 in Hg or 90 kPa was applied. Subsequently, the models were saturated with CO_2, and the entire procedure of vacuum – CO_2 saturation was repeated. Saturation of the models was facilitated using a methylcellulose solution. The achieved viscosity of the employed viscous fluid was 23 cP in all three performed experiments, as per the laws of similitude for centrifuge testing [14]. Close monitoring during the saturation process ensured that no dry pockets of soil were trapped in the stratum.

2.3. High-Speed camera monitoring

An assessment of the lateral surficial displacement of the deposits was achieved by image analysis of a high-speed camera (Phantom v5.1, produced by Vision Research) recording. The camera is permanently installed on the centrifuge beam cross-member, isolating the camera in this way from the basket vibrations [15]. Depending on the applied g-level, the camera is tilted by an appropriate angle, to provide a view directly perpendicular to the sloped soil surface. The sampling rate utilized for this series of experiments was 1000 frames per second in model scale (43.50 Hz in prototype).

On the deposit surface, a grid of zip tie heads was installed (Fig. 3) and tracked with the high-speed camera. Limitations, which had to do with light being reflected on the generated waves within the free standing water, did not allow tracking of the entire grid of targets but rather only the area included in the blue dashed frame of Fig. 3. The recording was triggered by the centrifuge data acquisition system, and thus the acquired recording was synchronized with the recordings of the buried sensors. As a reference Table 3 provides the coordinates of the targets, as they were measured during construction for RPI01 and replicated for RPI02 and RPI03, and as they were measured before dissection of the model for RPI01, RPI02 and RPI03.

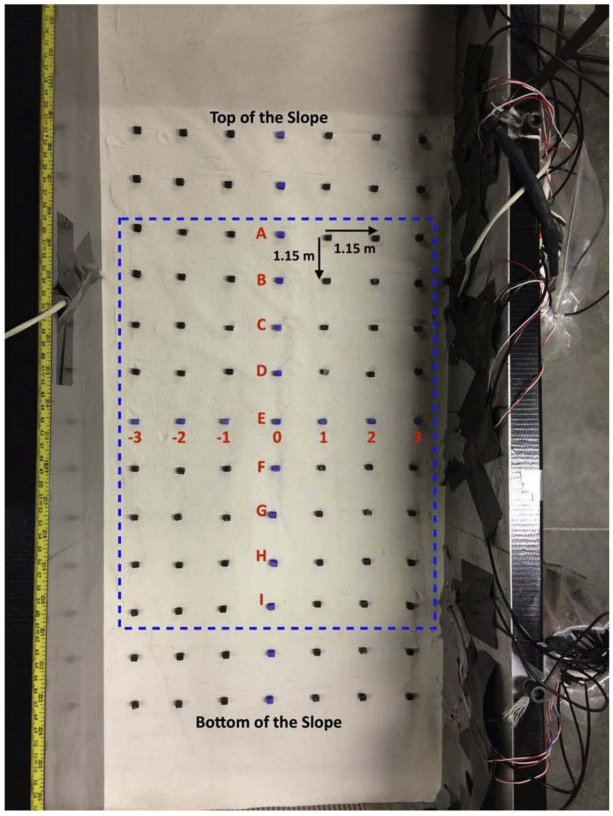

Fig. 3. Grid of targets used for tracking with the high-speed camera (the blue dashed frame indicates the area which was actually tracked). (For interpretation of the references to colour in this figure legend, the reader is referred to the Web version of this article.)

2.4. Testing sequence

The models were subjected to a series of synthetic ramped sinusoidal motions that constituted a sequence of non-destructive and destructive shakings. Table 4 provides an overview of the applied testing program. All motions had a predominant frequency at 1 Hz, but varied in amplitude. The amplitude of the 1st destructive shake was at 0.15 g and of the 2nd destructive shake was at 0.25 g. In this paper, only the results from the 1st destructive shake are presented and discussed. The RPI02 and RPI03 experiments included a CPT. In both cases, the CPT was performed before the first destructive shake. A CPT was also performed after the first destructive shake of the RPI02 test. Before and after each applied motion and each CPT, a bender element test was performed.

3. Experimental results

3.1. CPT and shear wave velocity

The relative density and shear wave velocity as measured before (Vs_b) and after (Vs_a) the first destructive shake, are presented in Table 5. The shear wave velocity was estimated by processing the data from the bender elements using the "first arrival" method, as it is described in Refs. [16–18]. A slight increase, in the order of 12% and 6%, is observed in RPI02 and RPI03 respectively. This general trend of the shear wave velocity increasing after a moderate ground motion, has also been observed by other researchers ([17,18]). Also in Table 5, a theoretical estimation of the expected shear wave velocity is presented, using the following two equations from [19,20]:

$$Vs = 13.18 * {q_c}^{0.192} * {\sigma'_{v0}}^{0.179}$$

$$Vs = 17.48 * q_c^{0.13} * \sigma_{v0}^{'0.27},$$

in which q_c and σ'_{v0} are expressed in kPa, giving Vs in m/s.

Both these methods are empirical correlations between the tip resistance from the CPT and the shear wave velocity and they confirm that the results of the bender elements and CPT are in good agreement. The obtained values of Vs yield a discrepancy of approximately 10% from the actually measured values. Table 6 shows the depth of the bender element blade, the respective effective stress and tip resistance at that location. The shear wave velocity normalized by the effective stress, $Vs1$, is shown also in Table 6, to enable a comparison of the shear wave

Table 4
Testing program for the RPI LEAP2017 centrifuge experiments.

Experiment	Non-Destr.1	CPT1	Destr. 1 (0.15 g)	CPT2	Destr. 2 (0.25 g)
RPI01	x	–	x	–	x
RPI02	x	x	x	x	x
RPI03	x	x	x	–	x

Table 5
Comparison of shear wave velocities (before Vs_b and after Vs_a shaking): (1) measured using bender elements and (2) estimated from CPT measurements.

Experiment	Dr (%)	Measured Vs_b (m/s)	Measured Vs_a (m/s)	Estimated Vs_b (m/)s	Estimated Vs_a (m/s)
RPI01	65%	–	–	–	–
RPI02	65%	129	145	117 [19] 127 [20]	118 [19] 127 [20]
RPI03	45%	118	125	95 [19] 110 [20]	–

Table 3
Locations of the surface tracking targets before the shaking for RPI01 and after the shaking for RPI01, RPI02 and RPI03 (z* is elevation of the targets measured from the bottom of the container).

	Before the Shaking:RPI01			After the Shaking: RPI01			RPI02		RPI03	
Target	x: m	y: m	z*: m	x: m	y: m	z*: m	x: m	z*: m	x: m	z*: m
	−6.61	−0.12	4.81	−6.38	−0.23	4.62	−6.38	4.60	−5.46	4.28
	−5.46	−0.12	4.69	−5.23	−0.23	4.49	−5.12	4.49	−4.31	4.28
A0	−4.31	−0.12	4.60	−4.08	−0.23	4.42	−3.97	4.37	−3.16	4.28
B0	−3.16	−0.12	4.51	−2.93	−0.23	4.32	−2.82	4.28	−1.67	4.23
C0	−2.01	−0.12	4.39	−1.67	−0.23	4.23	−1.54	4.19	−0.52	4.28
D0	−0.86	−0.12	4.30	−0.52	−0.23	4.14	−0.37	4.09	0.75	4.16
E0	0.29	−0.12	4.21	0.63	−0.12	4.07	0.85	4.03	1.67	4.14
F0	1.44	−0.12	4.12	1.78	−0.12	3.96	2.14	3.96	2.82	4.12
G0	2.59	−0.12	4.00	2.93	−0.12	3.89	3.32	3.89	3.97	4.05
H0	3.74	−0.12	3.91	4.08	−0.12	3.84	4.37	3.82	5.00	3.96
I0	4.89	−0.12	3.80	5.23	−0.12	3.77	5.54	3.77	6.04	3.96
	6.04	−0.12	3.66	6.38	−0.12	3.63	6.63	3.68	6.96	3.86
	7.19	−0.12	3.54	7.53	−0.12	3.54	7.65	3.54	7.99	3.77

Table 6
Cone tip resistance and normalized shear wave velocity at the depth location of the bender elements for the conducted centrifuge experiments.

Experiment	Depth (m)	Effective Stress σ' (kPa)	Vs1_b (m/s)	Vs1_a (m/s)	Measured Tip Resistance q_{c1} (MPa)	Measured Tip Resistance q_{c2} (MPa)
RPI01	–	–	–	–	–	–
RPI02	2.88	29.20	176	198	3.72	3.83
RPI03	2.99	28.77	161	171	1.28	–

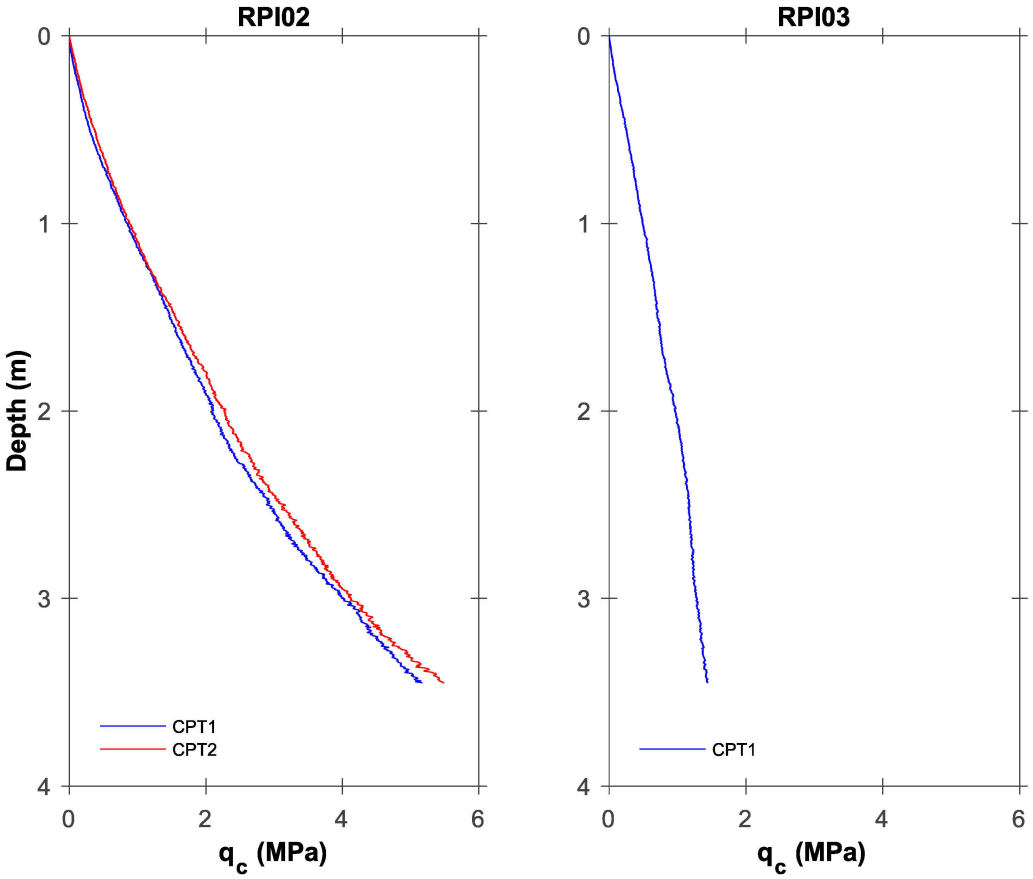

Fig. 4. CPT results showing the cone tip resistance for RPI02 (before and after the 1st destructive shake) and RPI03 (before the 1st destructive shake).

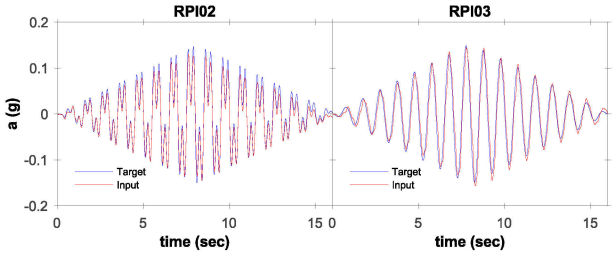

Fig. 5. Comparison between the input motion applied by the shaking table (average of AH11 and AH12) and the theoretical target ground motion.

velocity values consistent with the current practice; with:

$$Vs1 = Vs\sqrt[4]{\frac{101.25}{\sigma'_v}}$$

where 101.25 kPa is the pressure corresponding to 1 atm, σ'_v (kPa) is the effective stress as determined at the depth of the blade of the bender element and *Vs* (m/s) is the velocity measured by the bender elements.

The CPT results are shown in Fig. 4. The RPI02 CPT results reveal a slight change in soil strength after the shake and indicate no significant

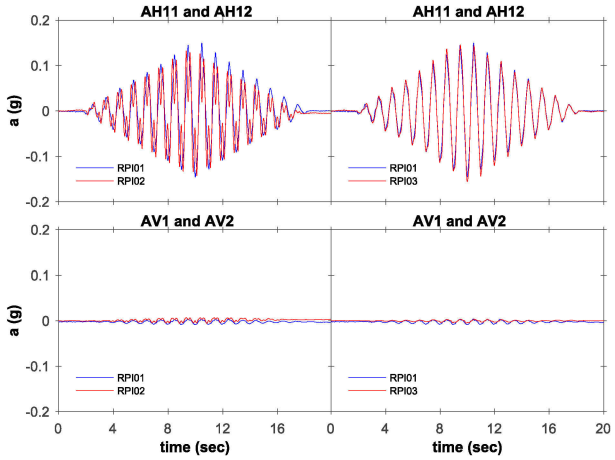

Fig. 6. Achieved input ground motion: average horizontal acceleration of AH11 and AH12 and average vertical accelerations of AV1 and AV2.

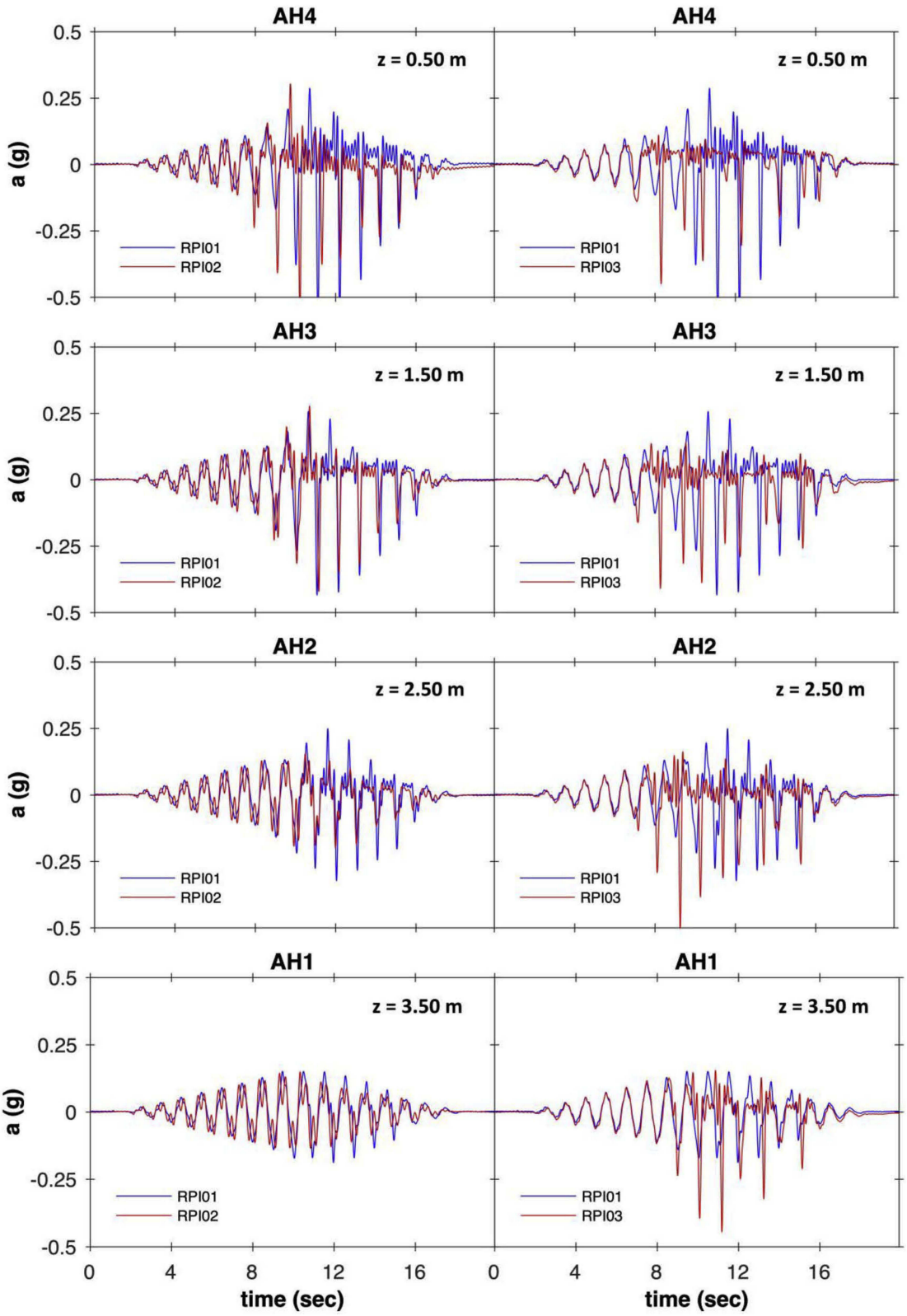

Fig. 7. Acceleration time histories along the central array.

change of the soil conditions. This finding is consistent with the slight increase in the shear wave velocity measured by bender elements (Table 5). The CPT results before the first destructive shake during RPI03 are approximately 66% lower than that of RPI02 and reflect the lower relative density. The almost linear shape of the CPT curves (Fig. 4), lacking any slope distortion, provides confidence in the obtained results and shows that the models were built with essentially a uniform relative density along the height direction.

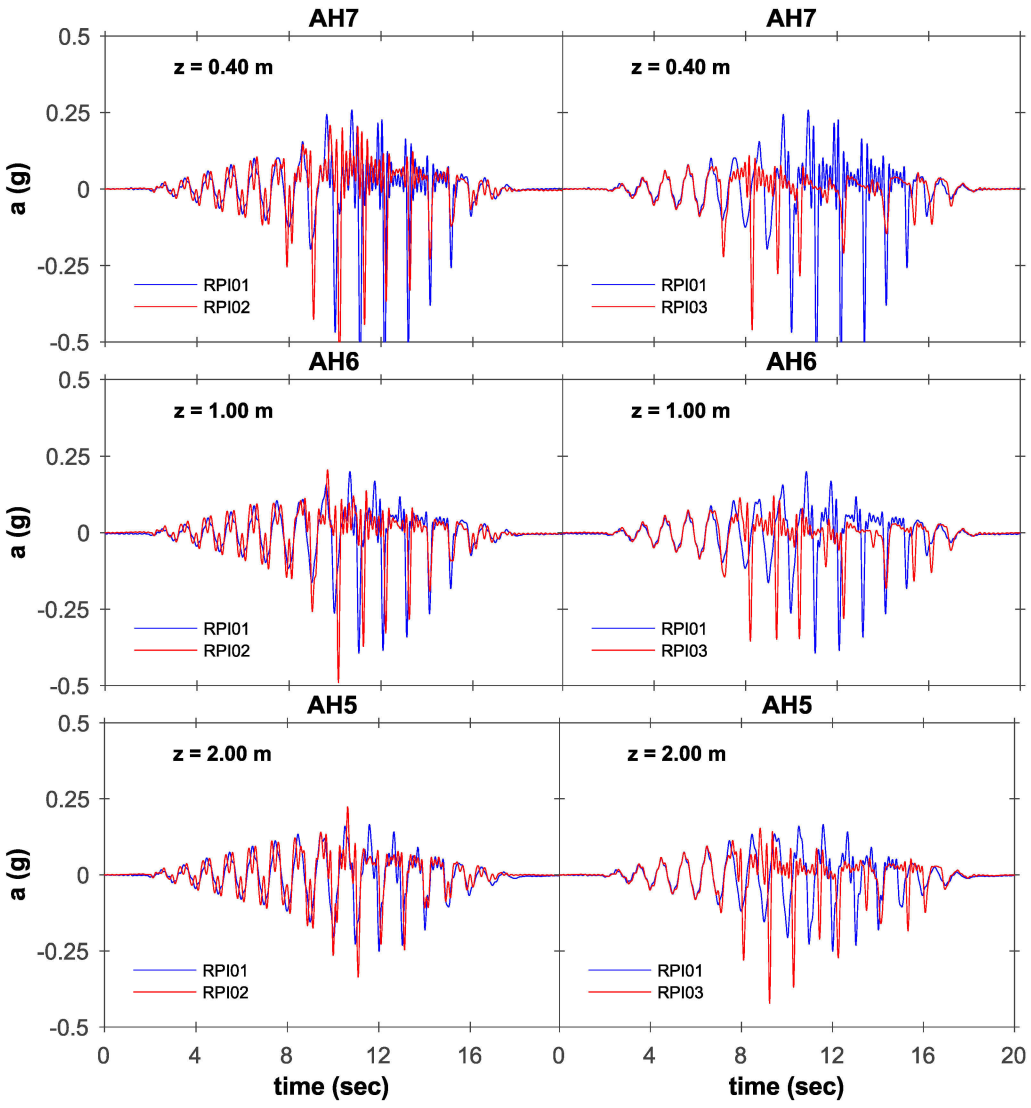

Fig. 8. Acceleration time histories along the upslope array.

3.2. Dynamic response

3.2.1. Accelerations

The LEAP-2017 set of tests was performed by applying a synthetic dynamic input motion of a sinusoidal shape with a tapered (increasing and then decreasing) intensity. Two different input types were used (Fig. 5). Type 1 had a single predominant frequency at 1 Hz (in prototype scale) and was utilized for RPI01 and RPI03. Type 2 had a predominant frequency at 1 Hz with an additional frequency component at 3 Hz and was utilized for RPI02 (Table 2). The addition of 3 Hz component aimed at assessing the effects of non-mono-frequency motions on the dynamic response. The presence of a 3 Hz component was a common feature among the different facilities participating in LEAP-2017. Fig. 5 shows a very good agreement between the target input motions and the ones actually applied by the centrifuge shaking table at the base of the models. Further assessment of the input motion quality is provided by Fig. 6, illustrating a comparison of the applied input motions for RPI01 - RPI02 and RPI01 - RPI03. RPI01 and RPI03 were performed with almost perfectly repeated input motions, which allows a comparison of these two tests in the certainty that the only major varying factor was the relative density. Fig. 6 also shows the averaged values from the accelerometers AV1 and AV2 recordings of the vertical acceleration during the experiments and confirms that no substantial additional rocking movement of the container took place during shaking.

Hereafter, the discussed experimental results include the central array of sensors as well as the upslope and downslope arrays. Along the central array, the soil conditions are less affected by the container rigid walls and resemble conditions of a shear column [21]. Figs. 7–9 show a comparison of the recorded accelerations of RPI01 and RPI02 and of RPI01 and RPI03. The accelerometer AH9 in the downslope array (Fig. 9) malfunctioned during RPI01 and RPI02.

The RPI01-RPI02 results reveal the effect of the additional frequency component in the input motion. The negative acceleration spikes of the RPI01 and RPI02 tests reflect the dilation response at large strains that occurred during the downslope motion and led to a temporary soil re-stiffening. This effect may have contributed to the observed large accelerations (at AH4, AH7 and AH10, Figs. 7–9) with peak values exceeding 200% of the peak input acceleration. De-amplification or low amplitude of the upslope (positive) acceleration values along the central array (Fig. 7) occurred after the onset of liquefaction at $t = 10s$ for $z = 0.50$ m. Deeper layers experienced liquefaction later than shallow strata, as the liquefied zone propagated downwards.

Interestingly, the addition of the 3 Hz component cycles apparently did not allow the soil grains to fully interlock and dilate, showing in this case a milder but still dilative behavior. The general trends for both

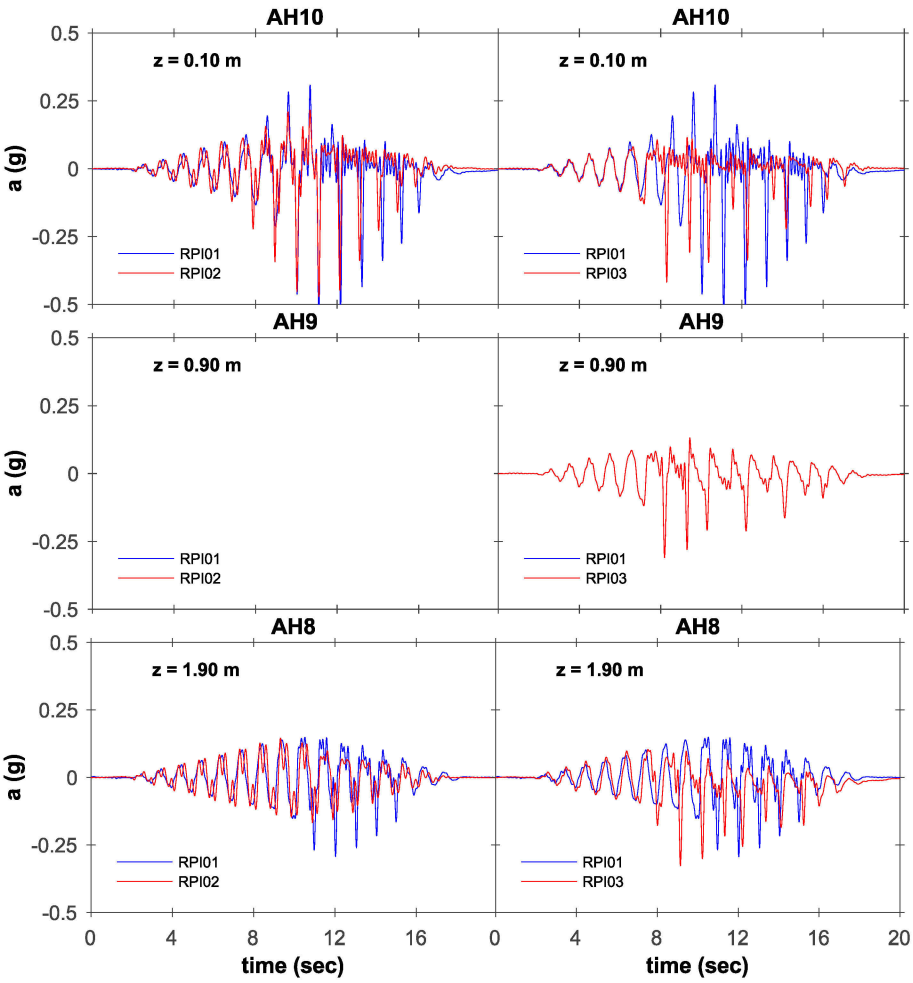

Fig. 9. Acceleration time histories along the downslope array.

models of RPI01 and RPI02 show good agreement. Liquefaction occurred and propagated practically simultaneously for RPI01 and RPI02. Note that the dilation spikes of these two tests coincide almost perfectly. The soil fabric of the two tests was similar and the presence of the 3 Hz component did not appear to affect in any significant fashion the timing of the dilation cycles.

The RPI01 and RPI02 responses along the upslope and downslope arrays (Figs. 8 and 9) are consistent with that of the central array. The dilative acceleration spikes of the upslope array (Fig. 8) have slightly smaller amplitude in the upper layers of RPI02 compared to RPI01. The additional frequency component apparently prevented the sand grains from fully interlocking and thus restricting the dilative response. This effect was also pronounced at the downslope locations AH8 and AH10 (Fig. 9).

The comparison between RPI01 and RPI03 reveals the soil response for two different relative densities (corresponding to medium dense and a loose soils) and consequently two different soil fabrics. There is a striking agreement between the two motions for all locations during the first few cycles (Figs. 7–9). For these cycles, the deformations are supposedly small, the soil has not liquefied yet and the two deposits demonstrate similar response. During the stronger shaking cycles, there is less agreement in the frequency content and amplitude. In the central array, significant de-amplification of the acceleration of RPI03 (Fig. 7) is observed in the upslope direction (positive acceleration values) starting approximately at t = 8s, due to liquefaction. A similar de-amplification is observed approximately at only t = 11s for RPI01. This time difference clearly shows that RPI03 liquefied earlier than RPI01. Strong dilation spikes (negative acceleration values) are evident in the RPI03 response along the entire depth of the stratum. These spikes are associated with large strains, as discussed below. After about 10s of shaking, the dilation spikes in the upper layers (AH3 – AH4) are somewhat smaller for RPI03 compared to RPI01. This is attributed to a more comprehensive liquefaction of RPI03, which reached all depths.

The two test accelerations were also marked by a phase difference. The asynchronous response in RPI03 is more evident towards the upper layers (AH2 - AH4 in Fig. 7). For these layers, the phase difference appeared at an earlier time compared to layers at greater depth (AH1). The phase lag in the RPI03 response is attributed to the soil being significantly loose, therefore having lower shear wave velocity and being more susceptible to liquefaction. In the liquefied upper zone the acceleration values (AH2 – AH4) are comparable for RPI01 and RPI03.

The upslope and downslope responses of RPI01 and RPI03 (Figs. 8 and 9) have similarities and differences with the central array. At location AH7 (top of the upslope array), the positive accelerations were de-amplified, as observed along the central array, indicating loss of soil strength due to liquefied conditions. The dilative negative acceleration spikes at this location decreased in amplitude after approximately 10s. The deeper layers of the upslope array (Fig. 8) exhibited strong dilative spikes throughout the shaking. The magnitude of the dilative acceleration spikes at AH5 (Fig. 8) are remarkably larger for RPI03 than the RPI02, which, as discussed below, is attributed to the higher strains experienced at this location. The downslope responses of RPI01 and RPI03 reveal a similar trend (Fig. 9), showing a decreasing magnitude of dilation at deeper layers.

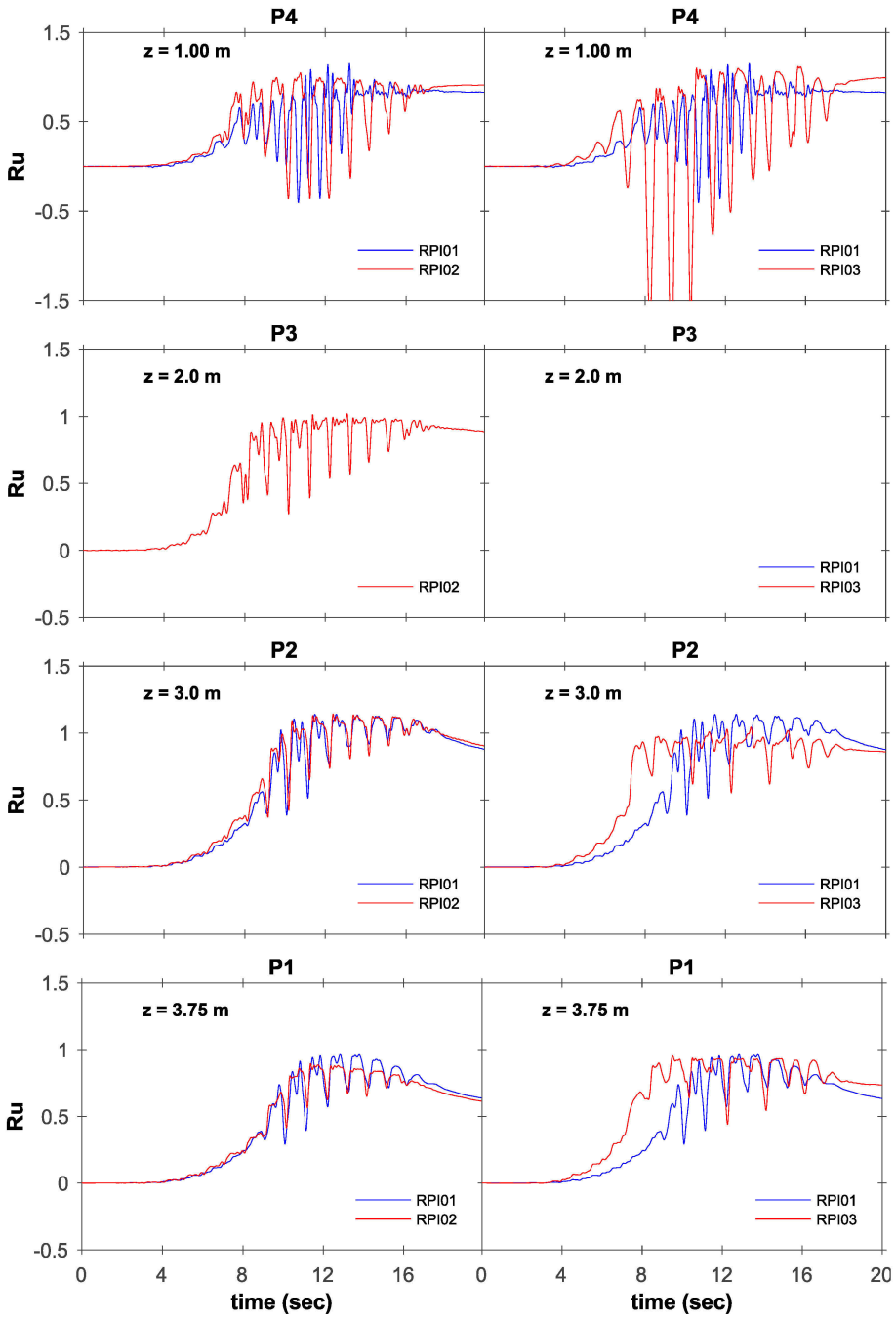

Fig. 10. Ru time histories along the central array.

3.2.2. Pore water pressures

The time history of the excess pore water pressure ratio of RPI02 and RPI03 are compared to RPI01 in Fig. 10 – Fig. 12 This ratio is defined as follows:

$$Ru = \frac{\Delta u}{\sigma_v^{'}}$$

where Δu is the excess pore water pressure and $\sigma_v^{'}$ is the vertical effective stress as evaluated before the shake.

The comparison between RPI01 and RPI02 in the central array (Fig. 10) shows strikingly good agreement of the recorded excess pore water pressures. The sensor P3 malfunctioned during RPI01, and only the RPI02 results are available for this location. The phase difference observed near the surface (P4) may be due to the sensor being placed at shallow depth and therefore being susceptible to the deposit motion because of the low confinement. This low confining pressure may also have contributed to the high dilative EPWP drops observed at this location. Note that the stratum experienced full liquefaction up to a depth of 3.00 m during shaking and reached a Ru of about 0.9 at 3.75 m depth (Fig. 10).

A comparison between the EPWP of RPI01 and RPI02 along the upslope and downslope arrays is presented in Figs. 11 and 12. Sensor P9 malfunctioned in RPI01 and P7 malfunctioned in RPI02. The upslope array exhibited large EPWP drops in the upper layer indicating strong dilation associated with the extension field created by the lateral downslope movement and deformation of the soil. The dilative spikes decreased significantly in amplitude in deeper layers. This is in agreement with the acceleration results (Figs. 7–9). The significantly lower dilation spikes attributed to the high frequency component observed in

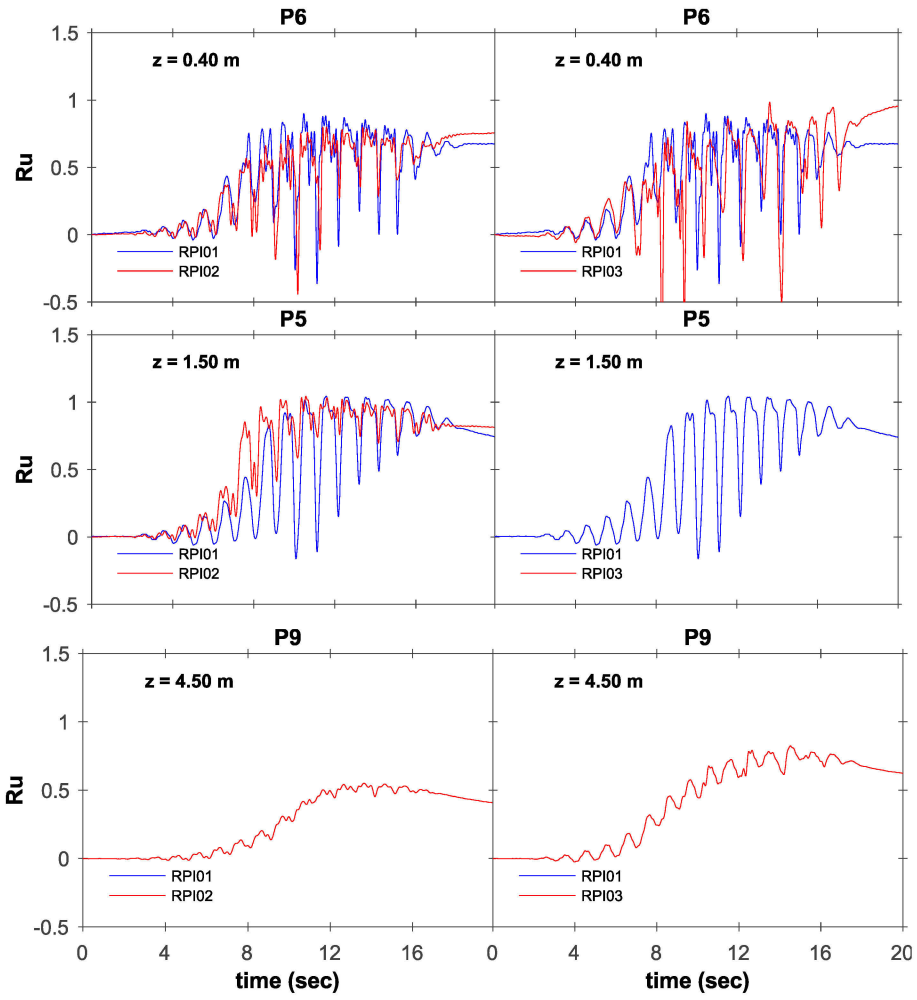

Fig. 11. Ru time histories along the upslope array.

RPI02 are also associated with lower EPWP drops, especially in upslope locations P6 and P5 (Fig. 11).

In general RPI01 and RPI02 show similar values of EPWP within all layers, upslope and downslope. In RPI02 in locations P9 (z = 4.50 m) and P10 (z = 3.20 m) reached Ru ≅ 0.60 (Figs. 11–12). In deeper layers the higher confinement allows higher capacity of EPWP to develop.

The comparison between RPI01 and RPI03 (Figs. 10–12) confirms the observations from the acceleration response. Sensors P3 and P5 malfunctioned for RPI03. Fig. 10 presents the comparison of the Ru response between RPI01 and RPI03 in the central array. Practically all locations indicate that the rate of pore pressure buildup was higher for RPI03, thus leading to liquefaction at an earlier stage compared to RPI01 (approximately at t = 8s for RPI03 and t = 11s for RPI01). The observed phase difference in Fig. 10 of the large dilation drops in pore pressure during the large cycles of shaking are consistent with the acceleration results. Moreover, in agreement with the acceleration results, the dilation drops in pore pressure tend to occur earlier and last longer for the upper layer of RPI03 compared to RPI01. The susceptibility of the looser deposit to liquefaction led also to significantly higher negative drops in EPWP in the upper layers (Figs. 10–12), associated with the high strains sustained by these layers, as discussed below.

Along the upslope locations, RPI01 and RPI03 show similar responses within the upper layer (Fig. 11). The deepest layer of the downslope array of RPI03 (P10) exhibited maximum Ru significantly higher than RPI02 (1.00 compared to 0.60). High EPWP built -up at a higher rate and propagated to greater depths during RPI03 underlining the higher susceptibility in liquefaction of the looser deposit. The downslope array (Fig. 12) showed trends similar to the ones observed in the central and upslope arrays.

3.3. Lateral displacements

The lateral surficial displacement of the slope (lateral spreading) was assessed by digital image analysis of the high-speed camera recording of the tracked targets. Two reference stationary points with a known distance between them, were selected on the rigid container. This distance provided the scale in the image analysis software to assess the displacements. The corresponding velocities and accelerations were obtained using time differentiation. Fig. 13 compares the acceleration obtained from tracking of a reference point on the rigid container with the recorded input motion of the centrifuge (for RPI02 and RPI03). This figure confirms the quality of the results obtained by image analysis [12], and show that tracking yielded reliable acceleration time histories in the presence of the high frequency component and the case of the loose soil deposit. A comparison between the accelerations of the central target E0 (Fig. 3) and accelerometer AH4 (located most adjacent to E0) is also presented in Fig. 13 and shows good agreement. Note that the dilation spikes during the stronger cycles of the motion were also captured successfully by the high - speed camera tracking. The image analysis produced some noise and mild distortion towards the end of the recordings. After the end of shaking at t = 16 s, the waves in the free standing water above the deposit affected the quality of tracking. Light reflected on the waves and obstructed the tracking of the targets. In this case, the obtained accelerations are shown with a dashed line (Fig. 13).

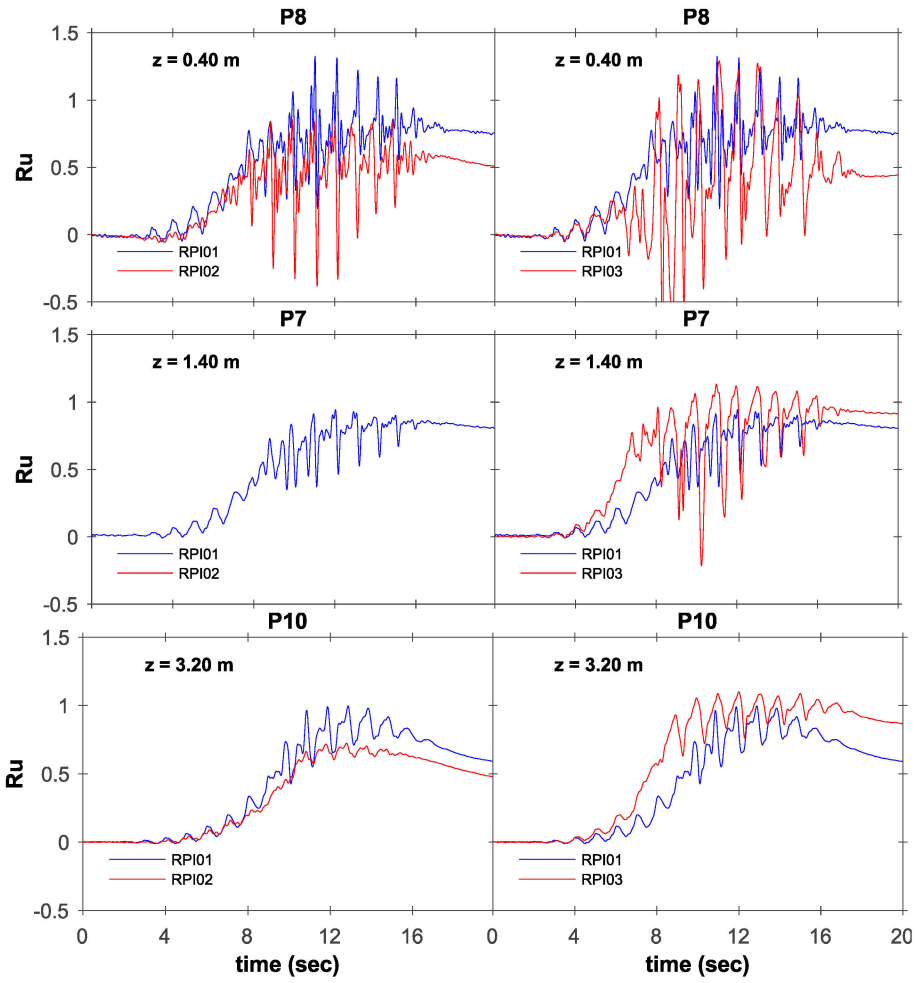

Fig. 12. Ru time histories along the downslope array.

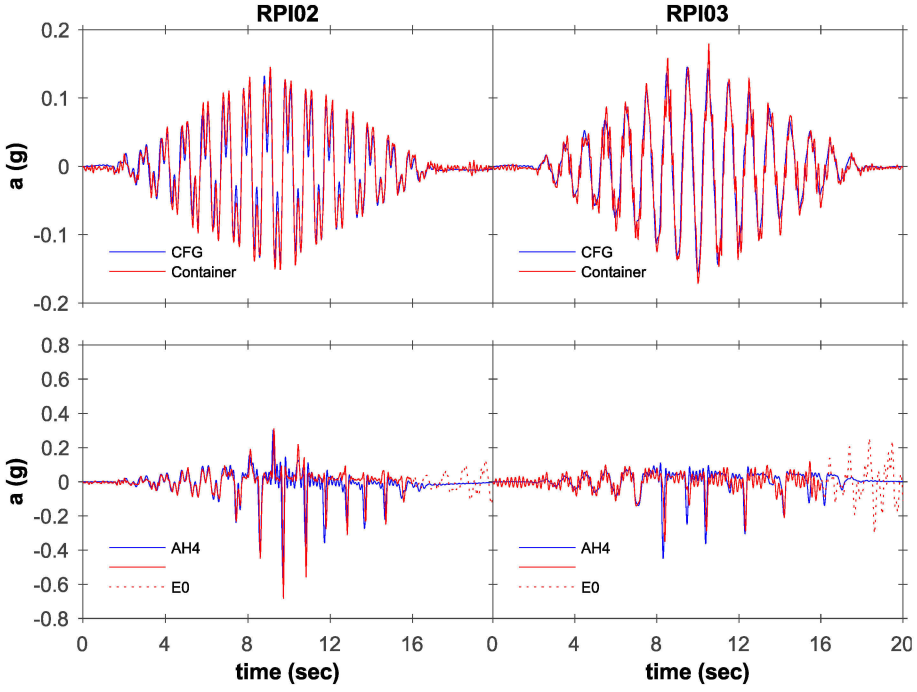

Fig. 13. Comparison between recorded accelerations and accelerations evaluated using high-speed camera tracking: (a) shaking table (CFG) and target on container, and (b) AH4 and target E0.

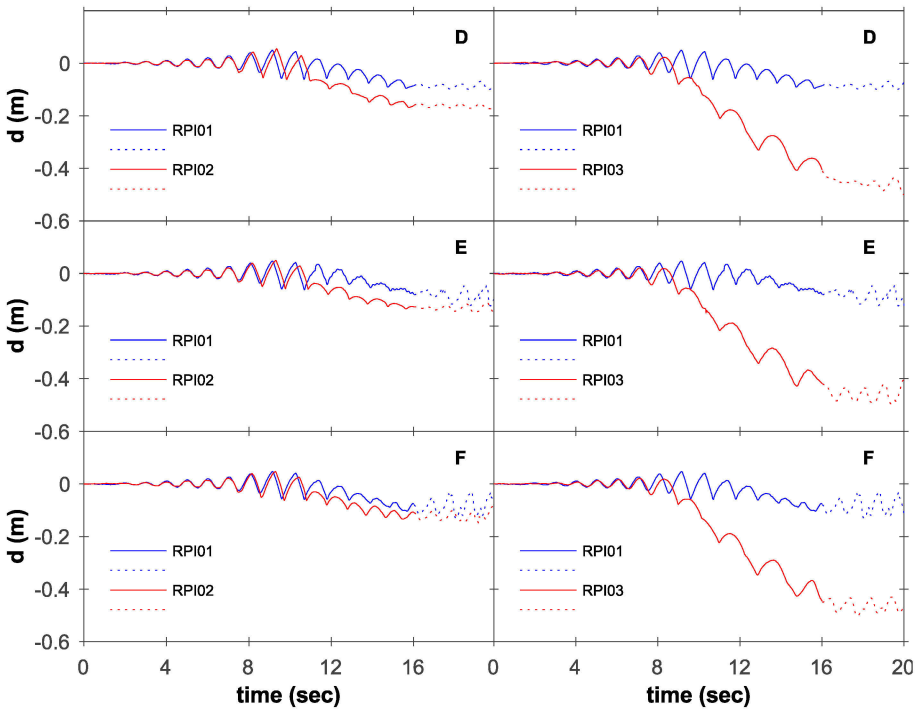

Fig. 14. Lateral surficial displacement time histories along the slope for LEAP-2017 (for targets D, E and F).

A comparison of the lateral displacement time histories of RPI01-RPI02 and RPI01-RPI03 is shown in Fig. 14. This figure shows the displacements of the targets D0, E0 and F0 along the central longitudinal axis (Fig. 3) to avoid results that may be affected by the boundaries. The displacement time histories in Fig. 14 are shown with dotted lines after the 16s time instant to indicate that the results are affected by wave interference noise (as discussed above). However, note that the permanent component of displacements was not affected by this complication.

The displacements of RPI01 and RPI02 are in very close agreement until t = 11 s (Fig. 14), which is the time when the excess pore water pressure ratio reaches the value 1.0 for both tests. However, the additional 3 Hz frequency component for RPI02 led to a slightly higher total lateral displacement (about 30%) by the end of shaking, which is attributed to a reduced soil interlocking during dilation, as discussed earlier.

The lateral displacement of RPI03 remained in close agreement with RPI01 until t = 8 s which also corresponds to the time when the excess pore water pressure ratio reached 1.0. Thereafter, RPI03 had a higher rate of accumulation of lateral displacements. The final value of lateral displacement for this test was almost four times higher compared to RPI01.

The horizontal and vertical coordinates of the targets provided in Table 3 were utilized to illustrate the shape of the slope surface before the shaking (Fig. 16). The shape of the slope in each of the tests after the dynamic event was obtained using physical measurements of the targets in x, y and z directions (Fig. 16). RPI01 and RPI02 exhibit similar shape after the end of shaking, with settlement at the top and middle of the slope and slight heaving at the bottom of the slope. RPI02 exceeded slightly the settlement and uplift values recorded in RPI01, which is in agreement with the lateral displacement results discussed earlier. RPI03 also showed significant heaving of the soil surface at the downslope side and leveling at the top of the slope (Fig. 16). The lower soil relative density and associated fabric account for these large displacements and heave. The shape of the slope after the end of the dynamic event is also depicted in Fig. 17.

4. Discussion and interpretations

The stress-strain response of the analyzed tests were determined from the acceleration time histories, as described in Ref. [22], and shown in Fig. 15 at different depths (z = 1.00 m, z = 2.00 m and z = 3.00 m) for RPI01, RPI02 and RPI03. The large drops in EPWP values observed during RPI01, RPI02 and RPI03 (Figs. 10–12) were found to correspond to the significant dilative response and associated stress peaks at large strains (Fig. 15). As the zone of liquefied soil propagated to deeper layers, higher strains, and thus stronger dilative Ru drops developed in the upper layers (shallower than about 2 m), as shown by P4, P6 and P8, as well as P3, P5 and P7. Furthermore, the relatively low confinement of P4, P6 and P8 may have also affected the response and contributed to the significantly higher EPWP drops at these locations (Fig. 10).

A comparison of the shear stress-strain response of RPI01 and RPI02 confirms the observations from the acceleration and Ru time histories. The downslope motion of the deposit introduced large strains, particularly at the middle and top of the slope, hence leading to significant dilatational stress spikes for both RPI01 and RPI02 (Figs. 7–8 and Fig. 15). However, the repeated change in the direction of shearing due to the 3 Hz frequency component, led to lower dilation and therefore higher strains in the upper layers of RPI02. At deeper layers (z = 3.0 m), the dilative response of RPI01 and RPI02 were comparable (Fig. 15), exhibiting lower shear strains. A comparison of stress-strain response of RPI01 and RPI03 shows opposite trends. Remarkably lower shear strains were developed in the upper layer during RPI03. Liquefaction reached deeper layers in this test leading to large strains within these layers, and appears to have prevented shear waves from propagating upwards. This isolation partly explains the reduction in amplitude of the dilatant acceleration peaks after the onset of liquefaction (Figs. 7–9). In contrast, the strong dilation spikes observed in the acceleration time histories AH1 and AH2 (Fig. 7) are associated with the deep layer high strains.

The susceptibility of the loose soil to liquefaction also led to large lateral surficial displacements, as shown in Fig. 14. The dynamic components of these lateral displacements had for RPI03 a period T ≅ 2s which is approximately double that of cycles of RPI01 (T ≅ 1s). The

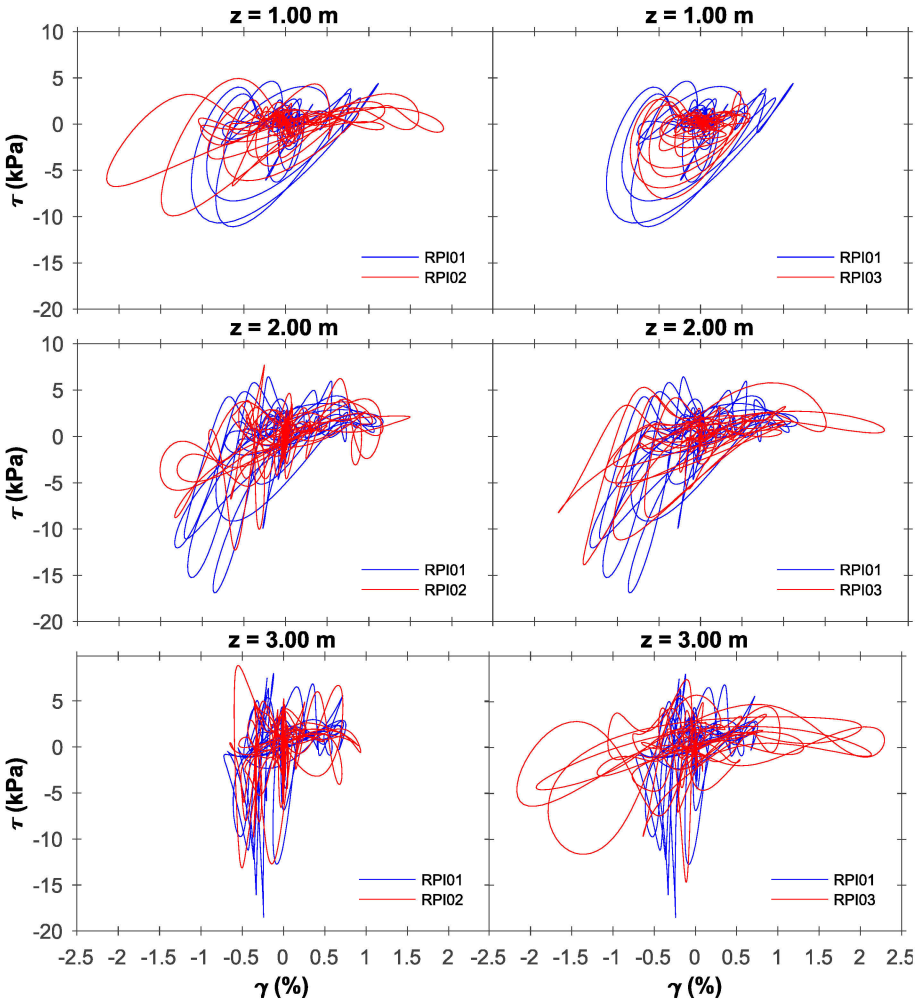

Fig. 15. Comparison of shear Stress - Strain response along the central array.

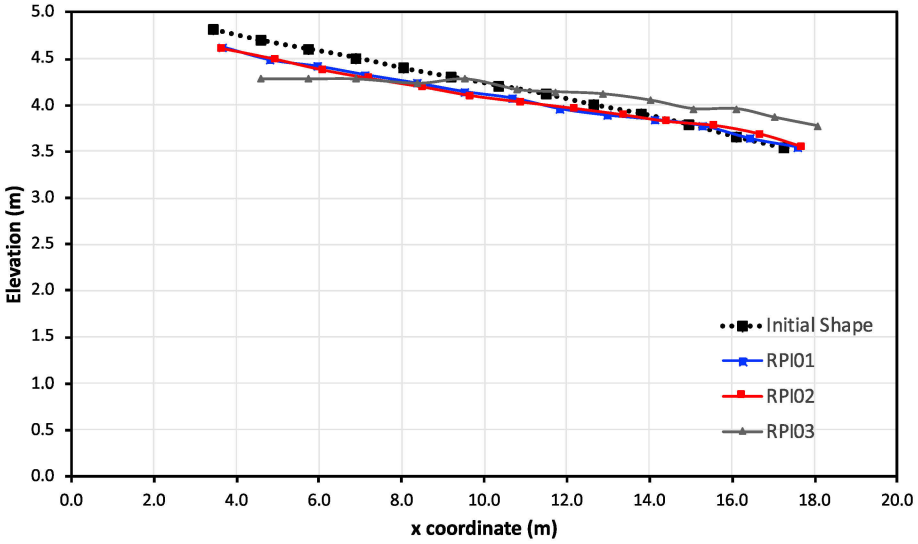

Fig. 16. Shape of the slope surface along the central array of targets before and after the shaking event.

predominant mechanism of lateral spreading in RPI03 is flow in the downslope direction, contrary to the mechanism of RPI01 and RPI02 which a significant cyclic 1 Hz component. Fig. 14 demonstrates that practically 100% of the lateral displacement occurred during the shaking phase. These observations are consistent with experimental results that were obtained during other studies, e.g. Ref. [4].

The recorded vertical displacement after shaking for RPI01, RPI02 and RPI03 are shown in Table 1 and Fig. 16. A settlement of the soil

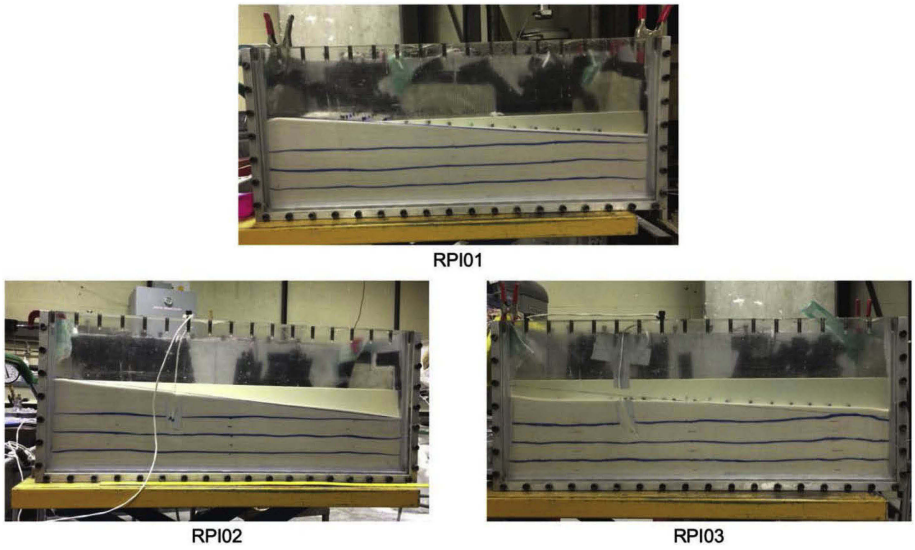

Fig. 17. Photos of the centrifuge models after the end of shaking.

deposit at the upslope and middle zones of the slope and uplift at the downslope zone were observed. The uplift is associated with heaving caused by the accumulation of soil permanent lateral spreading in the upslope and middle zones (Table 1) and the presence of the container (practically) rigid wall. RPI03 exhibited consistently the highest values of settlement and uplift at the downslope and upslope zones, respectively. This test had almost 4 times higher lateral permanent surficial displacements, and hence higher values of vertical displacements were expected.

5. Conclusions

The LEAP-2017 centrifuge model consisted of a saturated Ottawa F65 sand deposit with a 5-degree slope tested in a rigid box and subjected to a tapered input motion. Three tests, RPI01, RPI02 and RPI03, were conducted at Rensselaer. RPI02 had an input motion with an extra 3 Hz component and RPI03 had a lower relativity density compared to RPI01. CPTs were used for quality assurance and showed that the models were pluviated practically with a uniform relative density along the depth. The CPTs also showed that the soil strength was not significantly affected by shaking with a maximum acceleration of 0.15 g. Any densification occurring during shaking led to only slightly higher CPT tip resistance. Bender element test results showed that shear wave velocities are in agreement with the cone penetration test data.

The acceleration time histories of RPI02 had comparable amplitude to RPI01 with slightly lower dilation spikes, attributed to the additional frequency component of the motion preventing the soil grains from fully interlocking. This effect of the additional frequency component is also clearly shown in the stress strain response, revealing significantly higher strains in the upper soil layers (of RPI02), due to reduced dilation. The time histories of pore water pressure build-up for RPI01 and RPI02 were consistent, and had large EPWP drops associated with strong dilative response.

The RPI03 test showed good agreement with RPI01 during the early low-acceleration cycles. Significant differences and a phase lag were observed during the strong cycles of shaking. Excess pore water pressure Ru = 1.00 developed approximately 3s quicker in RPI03, lasted longer and propagated up to a depth of z ≅ 3.75 m. These differences are attributed to a higher susceptibility to liquefaction due to the lower relative density and associated looser soil fabric. On the other hand, the RPI01 and RPI02 denser soil deposits required more acceleration cycles (and therefore energy) to reach a pore ratio of 1.0, and consequently liquefied fully only up to 3.00 m depth. Thus, significantly higher strains were observed in RPI03 at larger depths (z = 3.00 m) than in RPI01 and RPI02. The upper layer of the liquefied zone is isolated from the lower layers of the deposit, exhibiting de-amplified acceleration values in the upslope direction and remarkably reduced shear strains.

Lateral spreading displacements were determined using image analysis of high-speed camera recordings. The quality of obtained displacements was verified and the displacement time histories revealed that RPI02 had slightly larger total permanent displacement (compared to RPI01), which is attributed to the lower dilation. In contrast, RPI03 had four times higher permanent lateral displacements in view of lower soil relative density. Lateral spreading in this test (RPI03) was governed by a low – frequency downslope flow, as opposed to the predominantly cyclic response in RPI01. The increased lateral deformations in RPI03 led to higher values of settlement and uplift at the top and bottom of the slope respectively.

Declaration of competing interest

The authors declare that they have no known competing financial interests or personal relationships that could have appeared to influence the work reported in this paper.

CRediT authorship contribution statement

Evangelia Korre: Investigation, Visualization, Formal analysis, Writing - original draft. **Tarek Abdoun:** Investigation, Validation, Formal analysis, Writing - review & editing. **Mourad Zeghal:** Conceptualization, Methodology, Funding acquisition, Formal analysis, Writing - review & editing.

Acknowledgements

The authors gratefully acknowledge the financial support of the National Science Foundation of USA (Grant No. CMMI-1635040 managed by Dr. Richard Fragaszy). The authors also express their appreciation to the staff of the Center for Earthquake Engineering Simulation at RPI for their vital support to the performance of the tests.

References

[1] Abdoun T, Dobry R, O'Rourke TD, Goh SH. Pile response to lateral spreads: centrifuge modeling. J Geotech Geoenviron Eng 2003;129(10):869–78.

[2] Dobry R, Thevanayagam S, Medina C, Bethapudi R, Elgamal A, Bennett V, et al. Mechanics of lateral spreading observed in a full-scale shake test. J Geotech Geoenviron Eng 2010;137(2):115–29.
[3] Elgamal A, Zeghal M, Taboada V, Dobry R. Analysis of site liquefaction and lateral spreading using centrifuge testing records. Soils Found 1996;36(2):111–21.
[4] Fiegel GL, Kutter BL. Liquefaction-induced lateral spreading of mildly sloping ground. Journal of geotechnical engineering 1994;120(12):2236–43.
[5] Ishihara K. Liquefaction and flow failure during earthquakes. Geotechnique 1993; 43(3):351–451.
[6] Lambe PC, Whitman RV. Dynamic centrifugal modeling of a horizontal dry sand layer. Journal of Geotechnical Engineering 1985;111(3):265–87.
[7] Zeghal M, Elgamal AW. Analysis of site liquefaction using earthquake records. Journal of Geotechnical Engineering 1994;120(6):996–1017.
[8] Perlea VG, Beaty MH. Corps of engineers' practice in the evaluation of seismic deformation of embankment dams. In: Proc., fifth international conference on recent advances in geotechnical earthquake engineering and soil dynamics, may 24-29, san diego. Special lecture SPL-6; 2010. p. 1–30.
[9] Arulanandan K, Scott RF. Verification of numerical procedures for the analysis of soil liquefaction problems. In: International conference on the verification of numerical procedures for the analysis of soil liquefaction problems (1993: davis, calif.). AA balkema; 1993.
[10] Manzari MT, Kutter BL, Zeghal M, Iai S, Tobita T, Madabhushi SPG, Zhou YG. LEAP projects: concept and challenges. In: Geotechnics for catastrophic flooding events - proceedings of the 4th international conference on geotechnical engineering for disaster mitigation and rehabilation, GEDMAR 2014; 2015.
[11] Kutter BL, Manzari MT, Zeghal M, editors. Model tests and numerical simulations of liquefaction and lateral spreading: LEAP-UCD-2017. Springer Open; 2019. https://doi.org/10.1007/978-3-030-22818-7.
[12] Korre E, Abdoun T, Zeghal M. Verification of the repeatability of soil liquefaction centrifuge testing at rensselaer." model tests and numerical simulations of liquefaction and lateral spreading: LEAP-UCD-2017. Springer Open; 2019. https://doi.org/10.1007/978-3-030-22818-7_19.
[13] Wei YC, Sasanakul I, Abdoun T. CPT-induced change of lateral earth pressure in modeling test. Int J Phys Model Geotech 2015;16(1):3–17.
[14] Taylor RE. Geotechnical centrifuge technology. CRC Press; 2014.
[15] Kokkali P, Abdoun T, Zeghal M. Physical modeling of soil liquefaction: overview of LEAP production test 1 at Rensselaer Polytechnic Institute. Soil Dynam Earthq Eng 2018. https://doi.org/10.1016/j.soildyn.2017.01.036.
[16] El-Sekelly W, Abdoun T, Dobry R. Soil characterization in centrifuge models through measurement of shear wave velocities using bender elements. In: GeoCongress 2012: state of the art and practice in geotechnical engineering; 2012. p. 2037–47.
[17] El-Sekelly W, Tessari A, Abdoun T. Shear wave velocity measurement in the centrifuge using bender elements. Geotech Test J 2014. https://doi.org/10.1520/GTJ20130189.
[18] El-Sekelly WE. The effect of seismic preshaking history on the liquefaction resistance of granular soil deposits. Rensselaer Polytechnic Institute; 2014.
[19] Hegazy YA, Mayne PW. October). Statistical correlations between vs and cone penetration data for different soil types. In: Proceedings of the international symposium on cone penetration testing, CPT, vol. 95; 1995. p. 173–8.
[20] Baldi G, Bellotti R, Ghionna VN, Jamiolkowski M, Lo Presti DCF. Modulus of sand from CPT and DMT. In: Proc. XII ICSMFE. Rio de Janeiro, august 13-18, 1989, vol. 1; 1989. p. 165–70.
[21] Zeghal M, Goswami N, Kutter BL, Manzari MT, Abdoun T, Arduino P, Ziotopoulou K. Stress-strain response of the LEAP-2015 centrifuge tests and numerical predictions. Soil Dynam Earthq Eng 2018. https://doi.org/10.1016/j.soildyn.2017.10.014.
[22] Zeghal M, Elgamal AW, Tang HT, Stepp JC. Lotung downhole array. II: evaluation of soil nonlinear properties. Journal of geotechnical engineering 1995;121(4): 363–78.